iScience

CellPress
OPEN ACCESS

Article

Selenium supplementation elevated SELENBP1 to inhibit fibroblast activation in pulmonary arterial hypertension

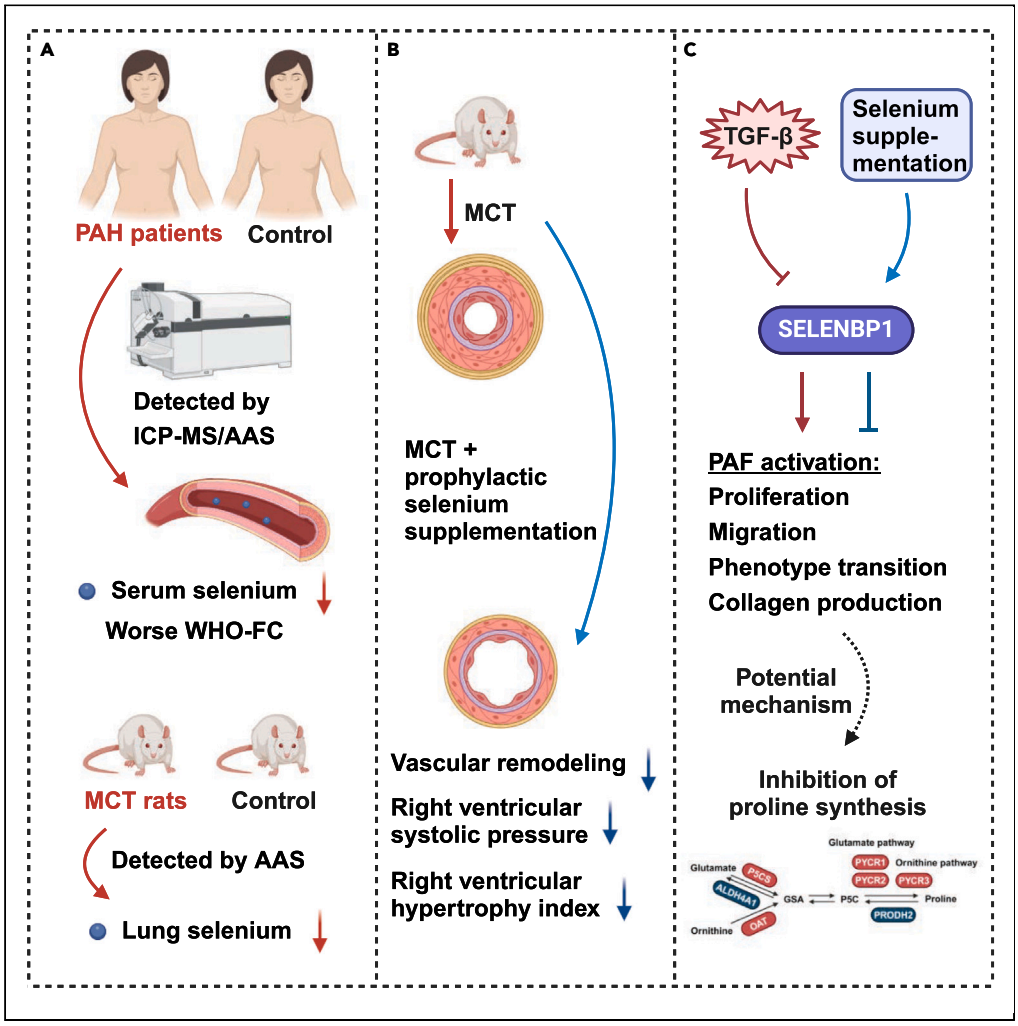

Benhui Liang, Wenchao Lin, Yiyang Tang, ..., Zaixin Yu, Lihuang Zha, Mengqiu Zhang

zhalihuang@csu.edu.cn (L.Z.)
821176847@qq.com (M.Z.)

Highlights

Selenium deficiency may be associated with the high risk and severity of PAH

Selenium supplementation effectively alleviated pulmonary hypertension in rat models

Selenium supplementation worked in a SELENBP1-dependent manner to inhibit PAF activation

Liang et al., iScience 27, 111036
October 18, 2024
https://doi.org/10.1016/j.isci.2024.111036

iScience

CellPress
OPEN ACCESS

Article

Selenium supplementation elevated SELENBP1 to inhibit fibroblast activation in pulmonary arterial hypertension

Benhui Liang,[1,2] Wenchao Lin,[2,3] Yiyang Tang,[1] Tangzhiming Li,[4] Qin Chen,[1] Wen Zhang,[5] Xinyi Zhou,[1] Jiayao Ma,[2] Boqing Liu,[6] Zaixin Yu,[1,2] Lihuang Zha,[1,2,7,*] and Mengqiu Zhang[1,2,*]

SUMMARY

Pulmonary arterial hypertension (PAH) is a life-threatening disease induced by abnormal activation of pulmonary adventitial fibroblasts (PAFs) in the early stage. The association between selenium deficiency and PAH is not yet fully understood. In this study, we found that the serum selenium content of PAH patients was significantly lower than that of healthy volunteers in two independent cohorts. Moreover, PAH patients with lower selenium levels may present poorer prognosis. Prophylactic selenium supplementation could effectively improve hemodynamics and pulmonary vascular remodeling in monocrotaline-induced pulmonary hypertension rat models. Mechanistically, selenium supplementation restored the level of selenium binding protein 1 (SELENBP1) which could exert an antagonistic effect on PAF activation. The rescue assay further proved that selenium supplementation worked in a SELENBP1-dependent manner. These findings demonstrated that selenium deficiency is an important risk factor in PAH, and the selenium-SELENBP1 axis represents a promising target for PAH prevention.

INTRODUCTION

Pulmonary arterial hypertension (PAH) is a deadly disease caused by genetic and environmental factors.[1] As the first group of pulmonary hypertension, PAH has the worst prognosis among all subtypes.[1,2] The median survival time of PAH patients without targeted therapy was only 2.8 years.[2] Even in this era of widely using PAH-targeted drugs, the long-term survival rate of the patients was still low.[3] With the development of PAH, irreversible pulmonary vascular remodeling was the obstacle that could not be overcome by existing drugs.[4] Thus, preventive treatment based on an in-depth understanding of the early pathogenesis of pulmonary vascular remodeling may be promising.

Evidence from PAH patients and animal models demonstrated that abnormal activation of pulmonary adventitial fibroblasts (PAFs) was an early driver of pulmonary vascular remodeling.[5–8] Under conditions such as external stress[6,7] or metabolic reprogramming of the cell itself,[8] PAFs underwent a phenotypic switch to myofibroblasts, enhancement of survival and migration, and secretion of collagen fibers and proinflammatory factors, which were known as activation of PAFs. These changes occurred in the early stage of PAH and resulted in excessive proliferation of pulmonary artery smooth muscle cells (PASMCs) and perivascular inflammation, ultimately promoting the development of pulmonary vascular remodeling.[5,7,9] Early inhibition of PAF activation was an effective means to reverse pulmonary vascular remodeling in animal models.[6–8] However, the etiology of PAF activation is not clear, and further studies are required to explore the pivotal targets for intervention.

The imbalance of trace elements is an important feature of PAH patients. Iron deficiency was a common clinical status in patients with PAH, and was closely related to their poor prognosis.[10] Iron deficiency led to spontaneous pulmonary vascular remodeling in rats, which may involve metabolic reprogramming and crosstalk with the BMPR2 pathway,[11,12] suggesting its role in the early pathological process of PAH. A small-scale pilot study found that the contents of copper, silver, chromium, and antimony in the circulation of PAH patients were significantly higher than those in healthy controls, which was positively correlated with the severity of the disease.[13,14] A nutritional investigation reported that the serum contents of selenium and SEPP1 in patients with systemic sclerosis-related PAH were significantly lower than those in healthy volunteers.[15] However, the role and mechanism of trace elements such as selenium in PAH and pulmonary vascular remodeling have not yet been fully elucidated.

[1]Department of Cardiology, Xiangya Hospital, Central South University, Changsha, Hunan, China
[2]National Clinical Research Center for Geriatric Disorders, Xiangya Hospital, Central South University, Changsha, Hunan, China
[3]Department of Nephrology, Xiangya Hospital, Central South University, Changsha, Hunan, China
[4]Department of Cardiology, Shenzhen People's Hospital, The First Affiliated Hospital of Southern University of Science and Technology, The Second Clinical Medical College of Jinan University, Guangzhou, Guangdong, China
[5]Department of Cardiology, Xiangya Third Hospital, Central South University, Changsha, Hunan, China
[6]Department of Clinical Medicine, Xiangya School of Medicine, Central South University, Changsha, Hunan, China
[7]Lead contact
*Correspondence: zhalihuang@csu.edu.cn (L.Z.), 821176847@qq.com (M.Z.)
https://doi.org/10.1016/j.isci.2024.111036

Recently, we screened the serum samples from PAH patients and healthy volunteers in our center by applying ionomic profiles, and found that the selenium level of PAH patients significantly declined in two independent cohorts. We further revealed by proteomics that the expression of selenium binding protein 1 (SELENBP1) was downregulated in PAH-related PAFs, which could be reverted by selenium supplementation. The purpose of this study was to explore the association between selenium level and the risk of PAH patients, and to clarify whether selenium participated in pulmonary vascular remodeling by regulating PAF activation through SELENBP1.

RESULTS

PAH patients had selenium deficiency, which correlated with the disease severity

This study recruited two independent PAH cohorts. The discovery cohort consisted of 78 PAH patients and 31 healthy volunteers, and the validation cohort consisted of 24 PAH patients and 15 healthy volunteers. Their clinical characteristics were shown in Tables S1 and S2, respectively. Using inductively coupled plasma mass spectrometry (ICP-MS) to screen the serum ionome of the discovery cohort, we found that the selenium content of PAH patients (median: 74.22, interquartile range: 58.14 to 94.68 μg/L) was significantly lower than that of healthy volunteers (median: 92.00, interquartile range: 80.77 to 113.00 μg/L), with $p < 0.05$ (Figure 1A). In the validation cohort, we confirmed the above conclusion through atomic absorption spectrometry (AAS) which was another ion quantitative analysis method (Figure 1B). Interestingly, after further distinguishing the subtypes of PAH, idiopathic PAH and hereditary PAH patients had the most obvious differences from healthy controls. Patients with other subtypes were no longer significantly associated with lower serum selenium content (Figures 1C and 1D). Moreover, linear regression analysis was conducted to determine the correlation between circulatory selenium content and some prognostic indicators of PAH. For the discovery cohort, the selenium content of PAH patients was significantly negatively correlated with their World Health Organization functional class (WHO-FC), with $r_{Pearson} = -0.358$ and $p = 0.001$ (Figure 1E). This association was also held in the validation cohort, with $r_{Pearson} = -0.493$ and $p = 0.014$ (Figure 1F). However, as shown in Figure S1, no statistical correlation was observed between selenium content and other indicators. These findings suggested that selenium deficiency may be associated with the high risk and severity of PAH.

Selenium supplementation effectively alleviated monocrotaline-induced pulmonary hypertension in rat models

To determine whether the selenium deficiency also existed in the pulmonary hypertension rodent models, we established monocrotaline (MCT)-induced rat models and MCT + selenium supplementation rat models (MCT+Se group). For the MCT+Se group, selenium-enriched water was supplied to each rat at the same time as MCT administration. As illustrated in Figure 2A, the lung selenium content of rats in the MCT group was significantly lower than that in control rats, while it was effectively rebounded in the MCT+Se group. For the phenotype of pulmonary hypertension, MCT rats had significantly higher right ventricular systolic pressure (RVSP) and right ventricular hypertrophy index (RVHI) than control rats, accompanied by severe pulmonary vascular remodeling. However, these rat models demonstrated significantly reduced RVSP and RVHI after prophylactic selenium supplementation, suggesting the improvement of pulmonary arterial pressure and right ventricular remodeling (Figures 2B and 2C). Further pathological staining of the lung sections confirmed that pulmonary arterial adventitial fibrosis and media hypertrophy were also reversed in the MCT+Se group (Figures 2D–2F). Our data clarified the important role of selenium in pulmonary circulation homeostasis.

SELENBP1 was significantly reduced in the pulmonary arterial adventitia of MCT rat models and PAF *in vitro* models

To elucidate the mechanism by which selenium supplementation could prevent PAH, we scanned the selenium-related proteins through proteomic profiles on pulmonary artery branches of MCT rats versus control rats. Proteomic data showed that protein abundance clustered well between the two groups (Figure 3A), with 257 upregulated proteins and 152 downregulated proteins. We then screened protein-coding genes with selenium relevance score ≥ 5 on the GeneCards website (Table S3)[16] and intersected these proteins with the differentially expressed proteins. SELENBP1 was the only candidate target (Figure 3B). Next, immunohistochemistry revealed that SELENBP1 was mainly expressed in the cells and extracellular matrix of the pulmonary arterial adventitia of control rats, while it was rarely expressed in MCT rats (Figures 3C and 3D). Western blot of lung proteins validated the finding (Figure 3E). As the primary cellular component of pulmonary arterial adventitia, rat PAFs were extracted and cultured to further investigate SELENBP1. The purity identification results of rat PAFs were shown in Figure S2. We stimulated PAFs by exogenous transforming growth factor β (TGF-β) to establish the *in vitro* model of pulmonary hypertension and found that the level of SELENBP1 in PAF models was also significantly decreased (Figure 3F).

Selenium supplementation restored the level of SELENBP1 and inhibited abnormal activation of PAFs

Compared with MCT rats, the expression of SELENBP1 in MCT+Se rats was significantly higher in both lung homogenate (Figure 4A) and pulmonary arterial adventitia (Figure 4B). Adding sodium selenite-enriched medium to TGF-β stimulated PAFs could also restore the level of SELENBP1, without obvious effects on normal cells (Figure 4C). More importantly, even after TGF-β stimulation, the expression of collagen-I, collagen-III, α-SMA, and PCNA in the PAFs with selenium supplementation was recovered to that of normal cells (Figure 4C), and the cell migration ability was also significantly decreased (Figure 4D), suggesting that selenium supplementation could effectively inhibit TGF-β induced PAF activation. However, for normal PAFs, selenium supplementation had no significant effect on the above phenotypes

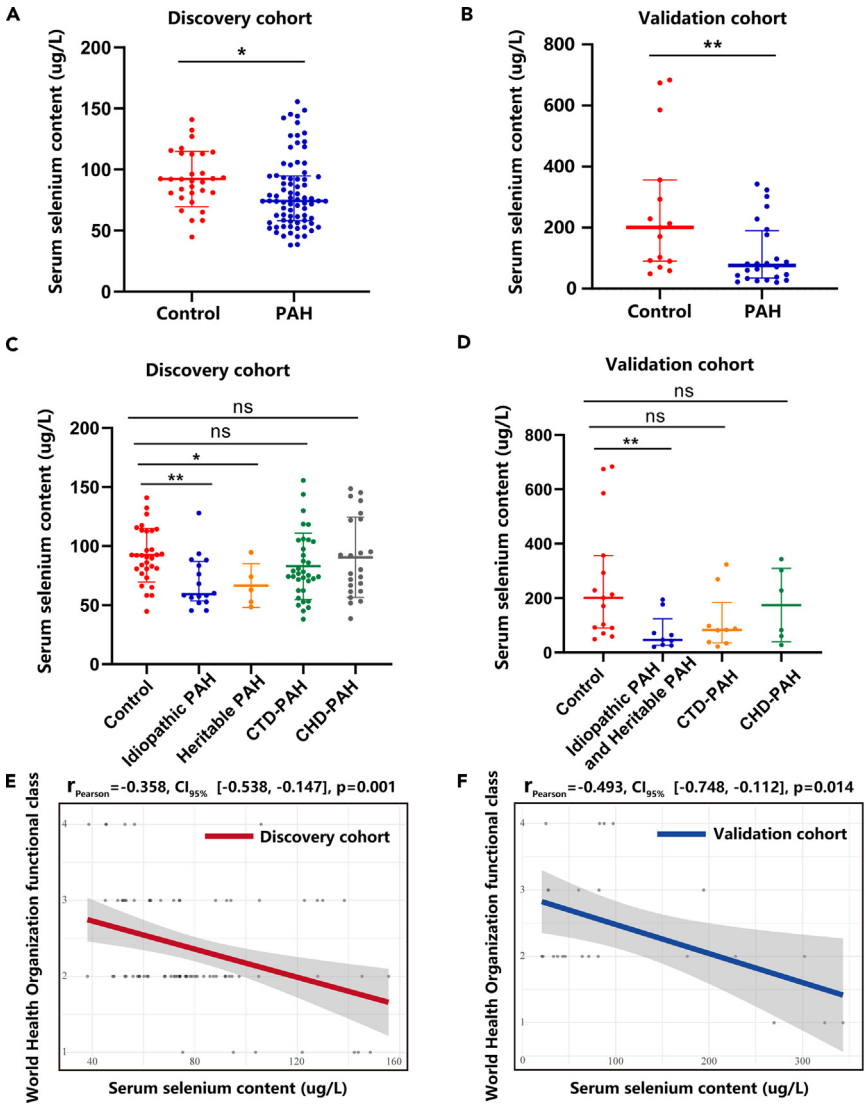

Figure 1. PAH patients had selenium deficiency, which correlated with the disease severity

(A) Serum selenium content of PAH patients (n = 78) and healthy controls (n = 31) in discovery cohort was determined by inductively coupled plasma mass spectrometry.

(B) Serum selenium content of PAH patients (n = 24) and healthy controls (n = 15) in validation cohort was determined by atomic absorption spectroscopy.

(C and D) serum selenium content in PAH patients of different subtypes in the discovery cohort and validation cohort, respectively.

(E and F) linear regression analysis of serum selenium content and World Health Organization functional class in PAH patients of discovery cohort and validation cohort, respectively. *, **, and ns indicate $p < 0.05$, $p < 0.01$, and no statistically significance, respectively. CTD, connective tissue disease; CHD, congenital heart disease.

except the collagen-III level. We also explored the potential impact of selenium supplementation on PASMCs. As shown in Figure S3, selenium supplementation reduced the viability of PASMCs in a dose-dependent manner.

Overexpression of SELENBP1 reversed PAF activation induced by TGF-β, while knockdown of SELENBP1 worsened the phenotype

To further determine the effect of SELENBP1 on PAFs, we transfected adenovirus vectors overexpressing SELENBP1 into PAFs. Transfection of empty adenovirus vectors into TGF-β stimulated PAFs had little effect on their activation, however, the phenotype transition to myofibroblasts, proliferation, migration, and collagen secretion of PAFs was significantly inhibited after overexpression of SELENBP1 (Figures 5A and 5B). In contrast, knockdown of SELENBP1 resulted in highly activated PAFs (Figures 5C and 5D). Our data proved that SELENBP1 functioned as a negative regulator of PAF activation.

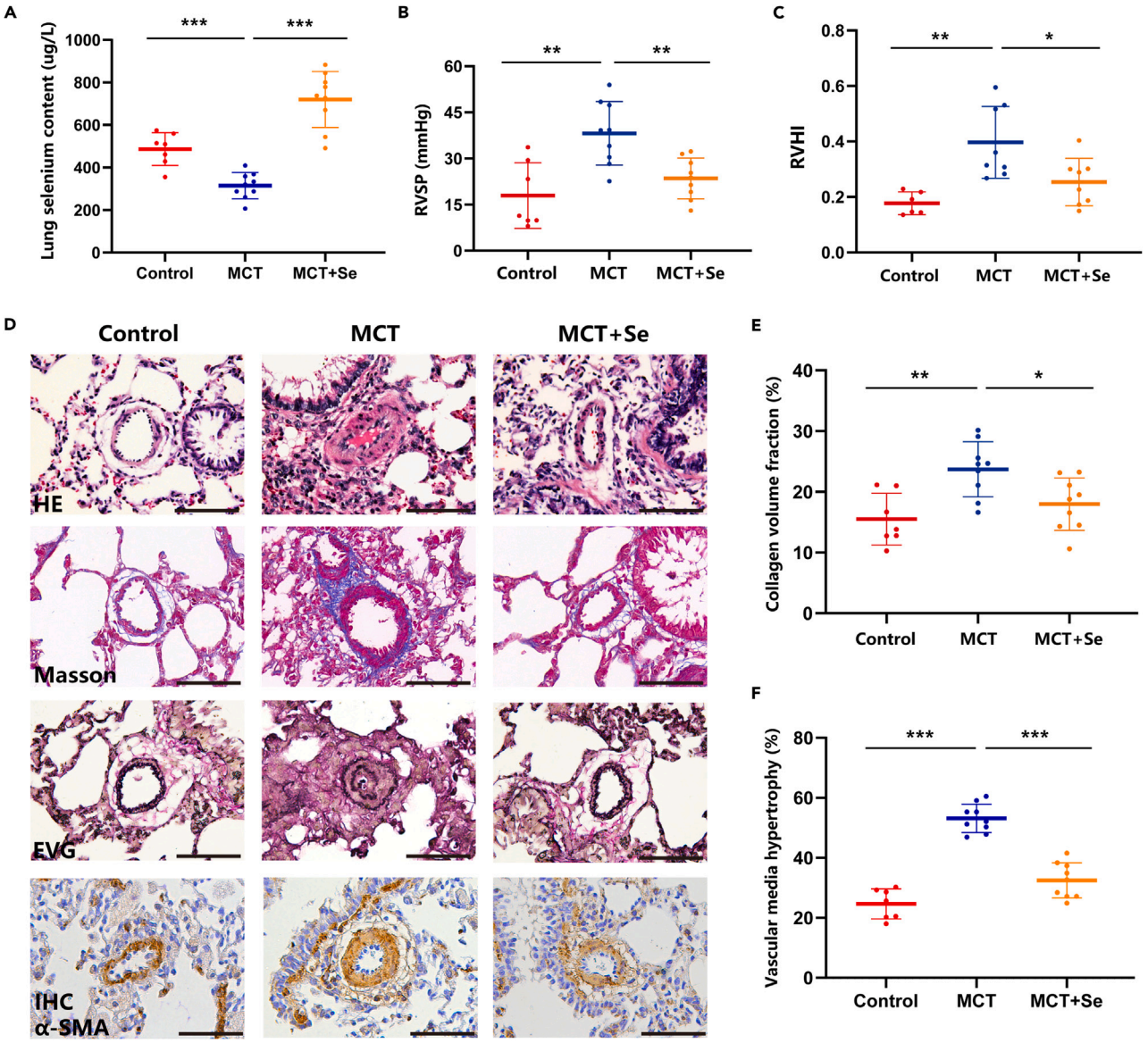

Figure 2. Selenium supplementation effectively alleviated monocrotaline-induced pulmonary hypertension in rat models

(A) Lung selenium content of control rats (n = 7), MCT rats (n = 9), and MCT+Se rats (n = 9) was determined by atomic absorption spectroscopy.

(B) RVSP of rats in these groups was determined by right heart catheterization.

(C) RVHI of rats in these groups was calculated by the weight of right ventricle/left ventricle+interventricular septum.

(D) Representative images of rats in these groups stained with HE kit, Masson's trichrome kit, EVG kit, and immunohistochemical probe for α-SMA (brown). Scale bar: 50 μm.

(E) Collagen volume fraction was represented as the percentage of collagen-positive area (blue) to the total area of pulmonary arterioles, which was calculated by ImageJ.

(F) Vascular media hypertrophy was represented as (arteriole diameter-lumen diameter)/arteriole diameter * 100%, which was calculated based on α-SMA stained images. *, **, and *** indicate $p < 0.05$, $p < 0.01$, and $p < 0.001$, respectively. Se, selenium supplementation; RVSP, right ventricular systolic pressure; RVHI, right ventricular hypertrophy index; HE, hematoxylin and eosin staining; EVG, Elastica van Gieson staining; IHC, immunohistochemistry.

Selenium supplementation inhibited PAF activation in a SELENBP1-dependent manner

Although both selenium supplementation and overexpression of SELENBP1 could effectively inhibit PAF activation, their effects may be independent. Therefore, we designed a convincing rescue assay that downregulated SELENBP1 after adding sodium selenite to the PAFs stimulated by TGF-β. Surprisingly, knockdown of SELENBP1 almost removed the beneficial effects of selenium supplementation on PAF activation (Figure 6).

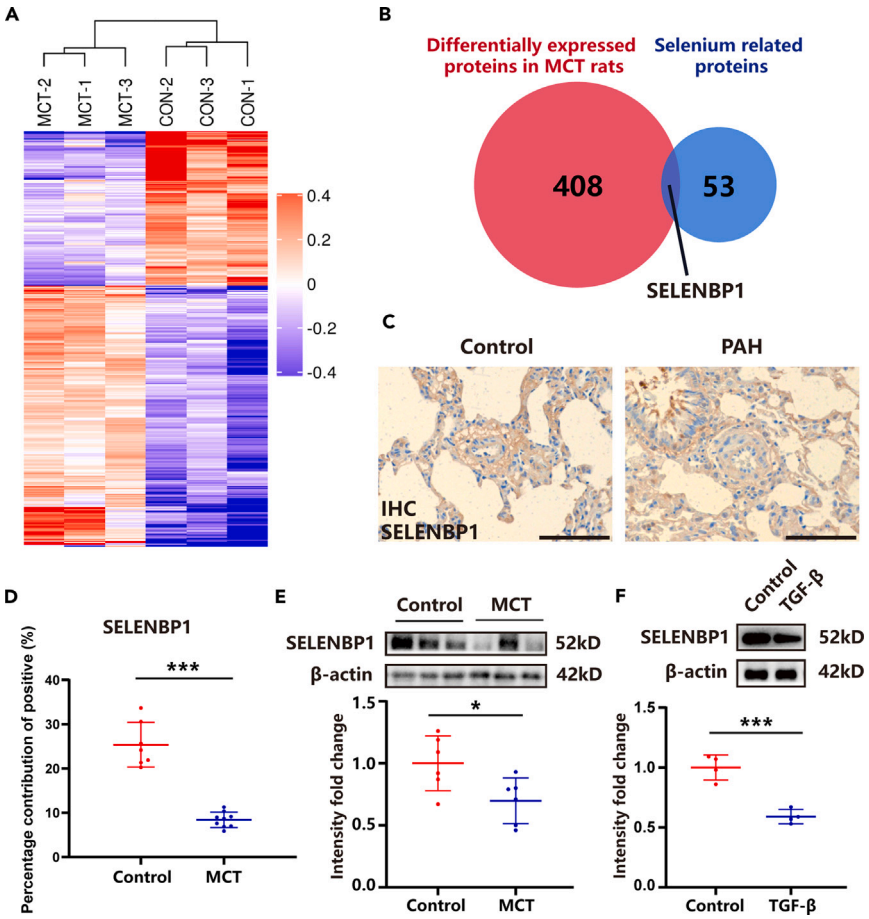

Figure 3. SELENBP1 was significantly reduced in the pulmonary arterial adventitia of MCT rat models and PAF *in vitro* models

(A) Cluster heatmap of differentially expressed proteins of pulmonary artery branches from MCT rats and control rats (n = 3) based on proteomics.

(B) Venn diagram obtained by the intersection of 409 differentially expressed proteins in proteomics and 54 selenium-related proteins in the GeneCards database.

(C) Representative images of MCT rats and control rats stained with the immunohistochemical probe for SELENBP1 (brown). Scale bar: 50 μm.

(D) For SELENBP1 staining intensity, the percentage contribution of positive in control rats (n = 7) and MCT rats (n = 9) was calculated based on the IHC Profiler plug-in component of ImageJ.

(E and F) Western blot and quantitative analysis of SELENBP1 in MCT group versus control group (n = 6) and TGF-β group versus control group (n = 4), respectively. * and *** indicate $p < 0.05$ and $p < 0.001$, respectively.

Selenium-SELENBP1 axis may inhibit PAF activation by downregulating proline synthesis

As illustrated in Figure 7A, the precursors of proline synthesis derive from the pathways of glutamate and ornithine, involving some essential synthases and lyases, which are necessary for collagen synthesis and PAF activation.[17,18] We detected the mRNA levels of the above enzymes after regulating the selenium-SELENBP1 axis, in which the expression of PRODH2 was too little to be detected. It was proved that selenium supplementation in TGF-β stimulated PAFs could significantly reduce the levels of P5CS, OAT, PYCR2, and PYCR3, but elevate the level of ALDH4A1 (Figure 7B). Overexpression of SELENBP1 could also decrease PYCR2 level and increase ALDH4A1 level, while knockdown of SELENBP1elevated P5CS and PYCR2 levels, but diminished ALDH4A1 level (Figures 7C and 7D). In the rescue assay, knockdown of SELENBP1 partially offset the effect of selenium supplementation on P5CS, PYCR2, and ALDH4A1 (Figure 7E).

DISCUSSION

In the past two decades, the understanding of iron deficiency in PAH patients has increased researchers' interest in other trace elements such as selenium. Selenium is one of the essential elements for the human body, which is mainly found in selenoproteins as the form of selenocysteine.[19] The major biological functions of selenium and selenoproteins include: (1) Constituting the antioxidant defense system and regulating reactive oxygen species; (2) Participating in immune response; (3) Regulating the metabolism and activity of thyroid hormone.[19,20] Severe selenium deficiency has been confirmed to be the cause of some endemic diseases such as Keshan disease and Kashin-Beck disease.[21]

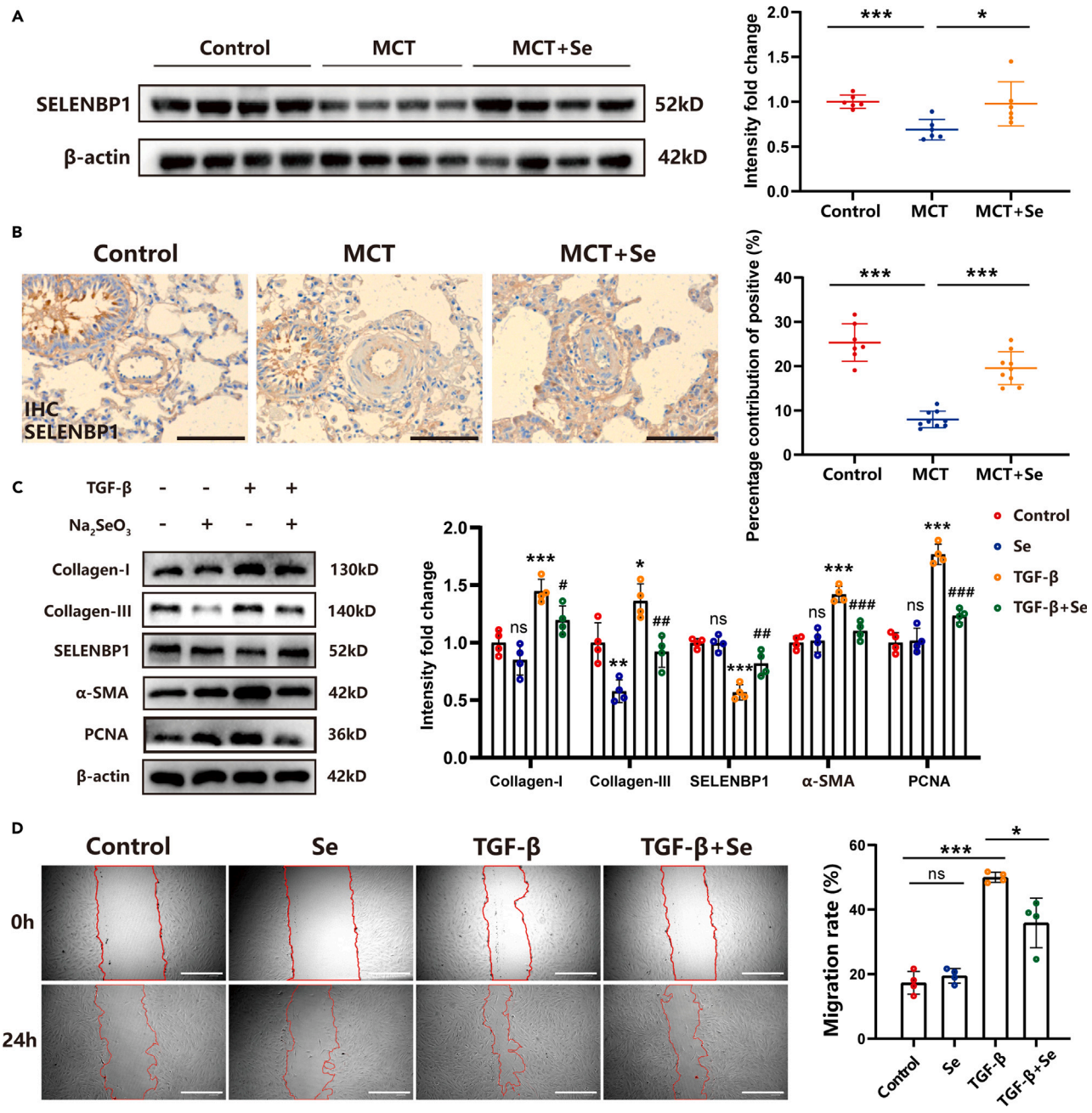

Figure 4. Selenium supplementation restored the level of SELENBP1 and inhibited abnormal activation of PAFs

(A) Western blot and quantitative analysis of SELENBP1 in control rats, MCT rats, and MCT+Se rats ($n = 6$).

(B) Representative images of control rats ($n = 7$), MCT rats ($n = 9$), and MCT+Se rats ($n = 9$) stained with the immunohistochemical probe for SELENBP1 (brown). Scale bar: 50 μm. The percentage contribution of positive was calculated to compare the differences.

(C) Western blot and quantitative analysis of indicated proteins in PAFs from the control group, Na_2SeO_3 group, TGF-β group, and TGF-β+Na_2SeO_3 group ($n = 4$). *, **, ***, and ns represent the comparation of Na_2SeO_3 or TGF-β group versus control group. ## and ### represent the comparation of TGF-β+Na_2SeO_3 group versus TGF-β group.

(D) Representative images of PAF scratches in the control group, Na_2SeO_3 group, TGF-β group, and TGF-β+Na_2SeO_3 group ($n = 4$) at 0 h and 24 h. The migration rate was represented as the percentage of the reduction of the same scratch width from 0 h to 24 h. Scale bar: 500 μm. *, ** (##), *** (###), and ns indicate $p < 0.05$, $p < 0.01$, $p < 0.001$, and no statistically significance, respectively. Na_2SeO_3, sodium selenite.

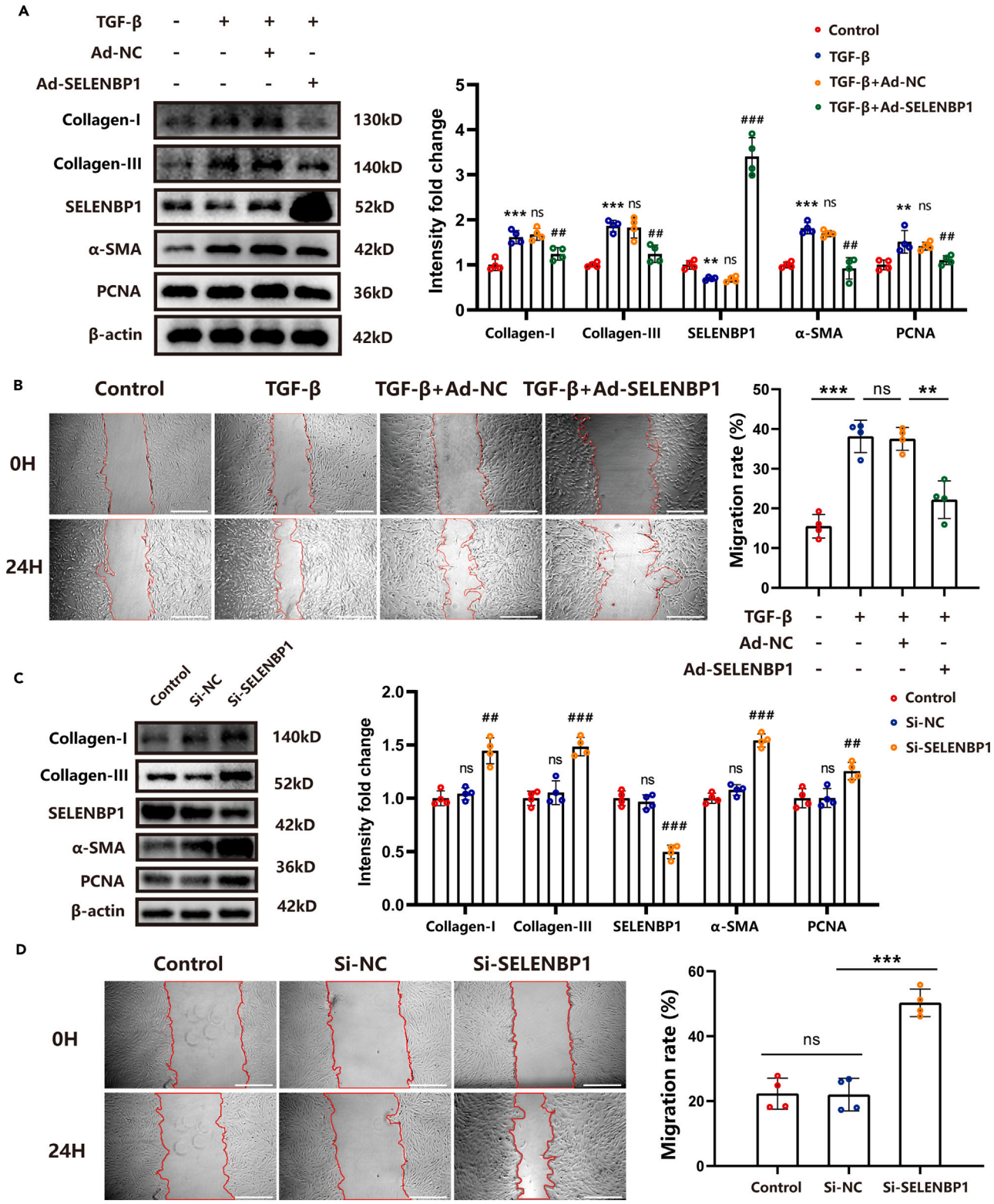

Figure 5. Overexpression of SELENBP1 reversed PAF activation induced by TGF-β, while knockdown of SELENBP1 worsened the phenotype

(A) Western blot and quantitative analysis of indicated proteins in PAFs from the control group, TGF-β group, TGF-β+Ad-NC group, and TGF-β+Ad-SELENBP1 group (n = 4). ** and *** represent the comparison of TGF-β group versus control group. Ns represent the comparison of TGF-β+Ad-NC group versus TGF-β group. ## and ### represent the comparation of TGF-β+Ad-SELENBP1 group versus TGF-β+Ad-NC group.

Figure 5. *Continued*

(B) Representative images of PAF scratches in control group, TGF-β group, TGF-β+Ad-NC group, and TGF-β+Ad-SELENBP1 group (n = 4) at 0 h and 24 h. The migration rate was calculated to compare the differences. Scale bar: 500 μm.

(C) Western blot and quantitative analysis of indicated proteins in PAFs from control group, Si-NC group, and Si-SELENBP1 group (n = 4). Ns represent the comparison of Si-NC group versus control group. ## and ### represent the comparation of Si-SELENBP1 group versus Si-NC group.

(D) Representative images of PAF scratches in control group, Si-NC group, and Si-SELENBP1 group (n = 4) at 0 h and 24 h. The migration rate was calculated to compare the differences. Scale bar: 500 μm. ** (##), *** (###), and ns indicate $p < 0.01$, $p < 0.001$, and no statistically significance, respectively. Ad-NC, empty adenovirus vector; Ad-SELENBP1, adenovirus vector carrying SELENBP1 expression sequence; Si-NC, negative control small interfering RNA; Si-SELENBP1, small interfering RNA targeting SELENBP1 mRNA.

Additionally, selenium deficiency was also associated with a high risk of chronic diseases such as coronary heart disease and various cancers.[19,20]

From bedside to bench, this study determined the relevance between serum selenium deficiency and high risk of PAH and further elucidated the role and mechanism of selenium supplementation in PAF activation. Compared with other investigations on the selenium nutritional status of PAH patients,[15,22] we more convincingly confirmed the association between serum selenium content and PAH through two independent PAH cohorts. ICP-MS and AAS are both mature ion quantitative analysis methods, in which ICP-MS is more suitable for high-throughput scanning of various ions in samples, while AAS is used for accurate quantitative analysis of a specific ion.[23] We found that the selenium content of PAH patients was significantly lower than that of healthy volunteers. Interestingly, low selenium content tended to be a feature of patients with idiopathic PAH or hereditary PAH. It formed a hypothesis that, beyond our understanding, the patients may

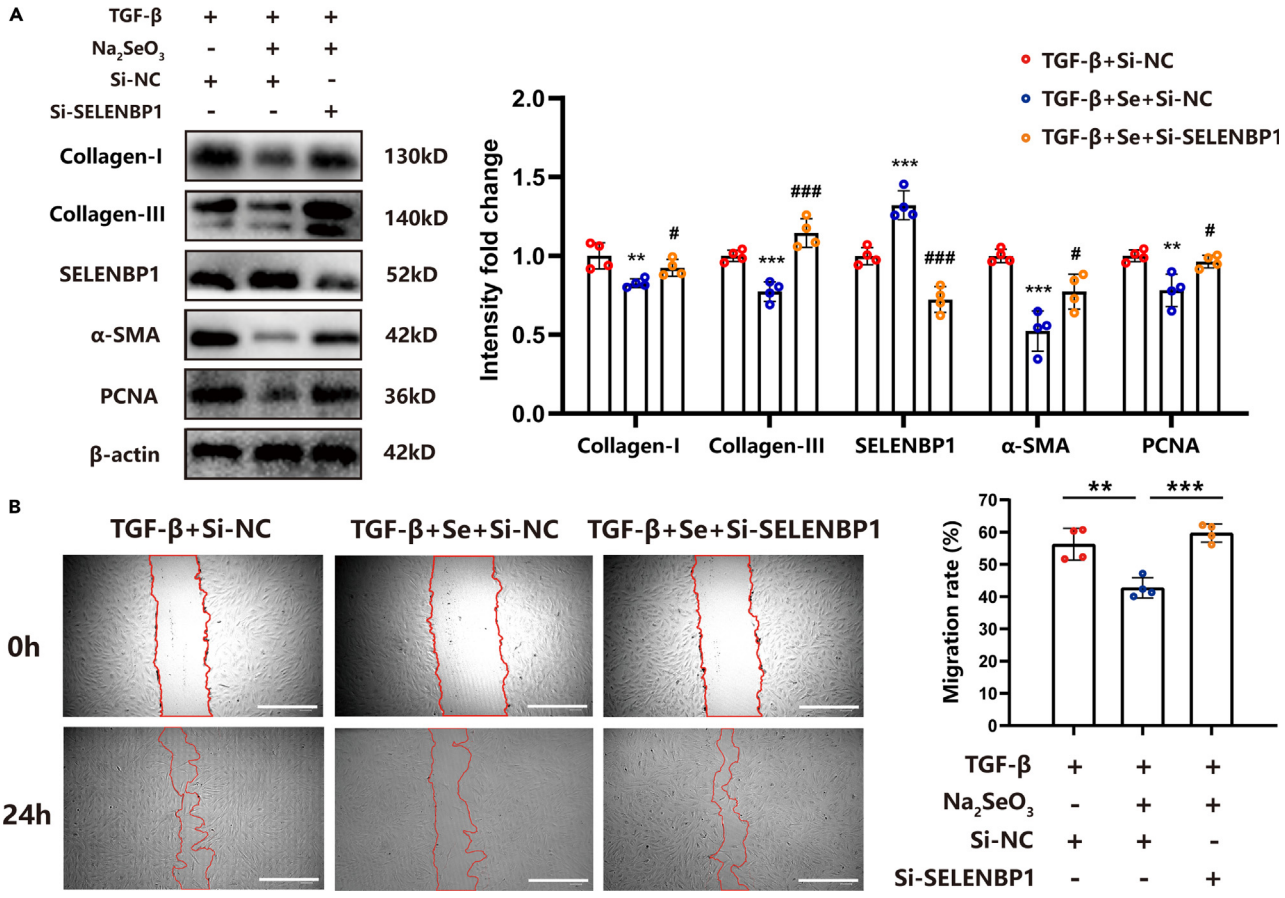

Figure 6. Selenium supplementation inhibited PAF activation in a SELENBP1-dependent manner

(A) Western blot and quantitative analysis of indicated proteins in PAFs from TGF-β+Si-NC group, TGF-β+Na_2SeO_3+Si-NC group, and TGF-β+Na_2SeO_3+Si-SELENBP1 group (n = 4). ** and *** represent the comparation of TGF-β+Na_2SeO_3+Si-NC group versus TGF-β+Si-NC group. # and ### represent the comparation of TGF-β+Na_2SeO_3+Si-SELENBP1 group versus TGF-β+Na_2SeO_3+Si-NC group.

(B) Representative images of PAF scratches in the above three groups (n = 4) at 0 h and 24 h. The migration rate was calculated to compare the differences. Scale bar: 500 μm. #, **, and *** (###) indicate $p < 0.05$, $p < 0.01$, and $p < 0.001$, respectively.

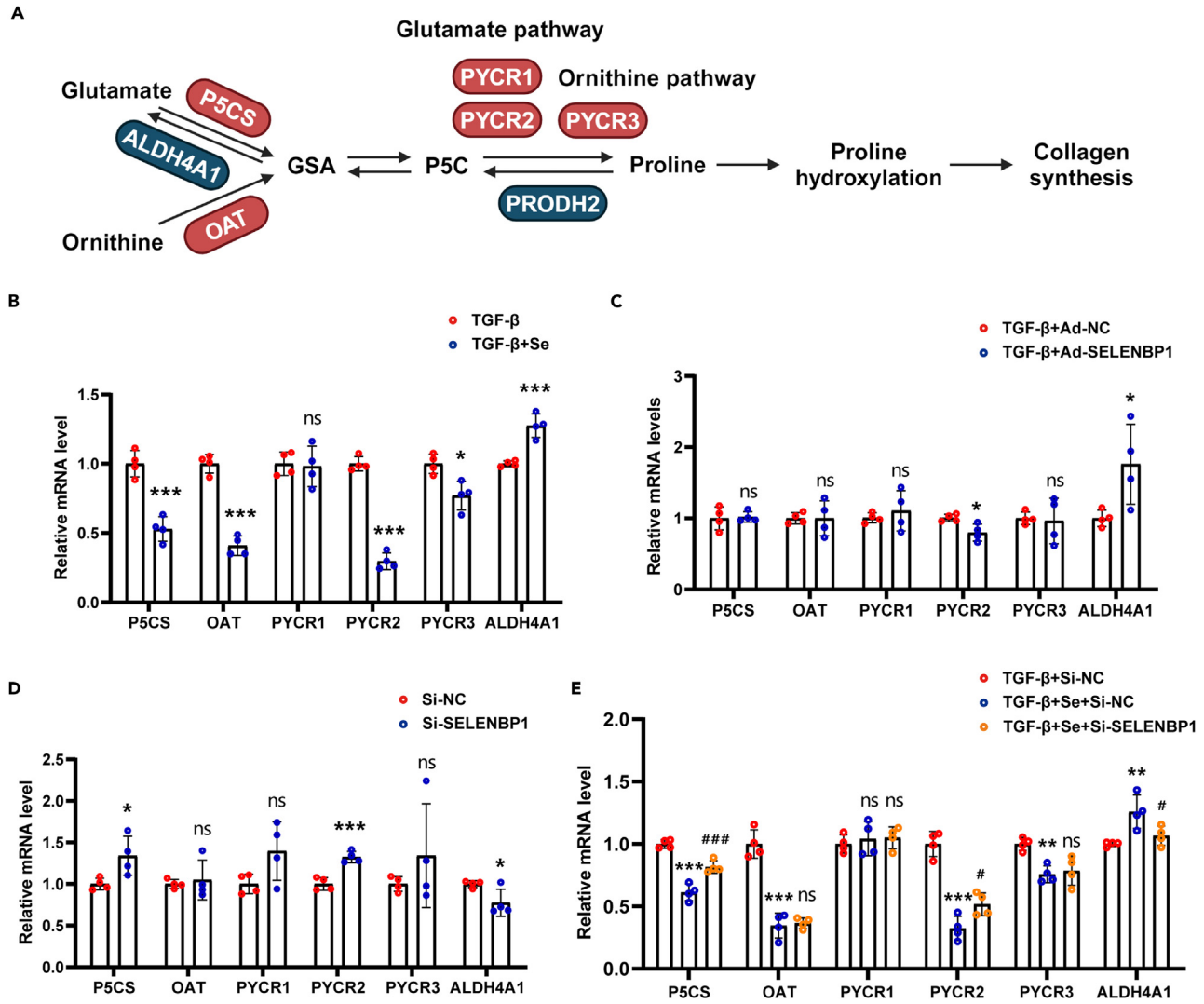

Figure 7. Selenium-SELENBP1 axis may inhibit PAF activation by downregulating proline synthesis

(A) The model diagram of proline synthesis pathway from glutamate and ornithine (the red label represents the key synthases) and proline degradation pathway (the blue label represents the key lyases).

(B) The PCR quantitative analysis of indicated genes in PAFs from TGF-β group and TGF-β+Na_2SeO_3 group ($n = 4$). *, ***, and ns indicate $p < 0.05$, $p < 0.001$, and no statistically significance, respectively.

(C) The PCR quantitative analysis of indicated genes in PAFs from TGF-β+Ad-NC group and TGF-β+Ad-SELENBP1 group ($n = 4$). * and ns indicate $p < 0.05$ and no statistically significance, respectively.

(D) The PCR quantitative analysis of indicated genes in PAFs from Si-NC group and Si-SELENBP1 group ($n = 4$). *, ***, and ns indicate $p < 0.05$, $p < 0.001$, and no statistically significance, respectively.

(E) The PCR quantitative analysis of indicated genes in PAFs from TGF-β+Si-NC group, TGF-β+Se+Si-NC group, and TGF-β+Se+Si-SELENBP1 group ($n = 4$). ** and *** represent the comparison of TGF-β+Se+Si-NC group versus TGF-β+Si-NC group. # and ### represent the comparation of TGF-β+Se+Si-SELENBP1 group versus TGF-β+Se+Si-NC group. #, **, *** (###), and ns indicate $p < 0.05$, $p < 0.01$, $p < 0.001$, and no statistically significance, respectively. P5CS, pyrroline-5-carboxylate synthetase; OAT, ornithine aminotransferase; PYCR1, pyrroline-5-carboxylate reductase 1; PYCR2, pyrroline-5-carboxylate reductase 2; PYCR3, pyrroline-5-carboxylate reductase 3; ALDH4A1, aldehyde dehydrogenase 4 family member A1; PRODH2, proline dehydrogenase 2.

have mutations in the pivotal genes regulating selenium metabolism, leading to selenium deficiency which further promoted the development of PAH. Considering the complicated process of selenium uptake, modification, transport, storage, and excretion, it is challenging to answer why selenium decreases. Clinical parameters are recognized as a key part of evaluating patients with PAH. According to guideline,[1] WHO-FC is one of the strongest predictors of survival in patients with PAH, both at diagnosis and follow-up. In this study, we collected the above clinical parameters of PAH patients at the first visit and found that PAH patients with lower selenium levels were associated with worse

WHO-FC, which may predict their clinical deterioration. However, no significant correlation between selenium content and other indicators was observed, which may be limited by the small sample size of this study.

After observing the selenium deficiency in PAH patients, we sought to understand how selenium affected PAH. Selenium deficiency also presented in the lung of MCT rats. Organic selenium supplements with higher bioavailability and safety than selenite were used in animal models. The hemodynamics and pulmonary vascular remodeling of these rats were significantly improved. Although some previous studies have investigated the therapeutic effect of selenium supplementation,[24–26] they mainly focused on observing the performance of animal models after treatment and lacked in-depth exploration of underlying mechanisms. In this study, we adopted proteomics to identify downstream targets mediating the biological function of selenium and ultimately selected SELENBP1. Unlike most selenoproteins, SELENBP1 did not have an active center containing selenocysteine, but could covalently bind selenite through a cysteine residue at site 57.[27] Our data demonstrated that SELENBP1 was a selenium-sensitive protein because selenium supplementation could restore SELENBP1 levels in MCT rats and TGF-β stimulated PAFs. SELENBP1 was mainly expressed in the cells and extracellular matrix of pulmonary arterial adventitia, which may be closely related to the most abundant PAFs in the adventitia. Thus, we further detected the activation level of PAF *in vitro* models after supplementing selenium or manipulating the expression of SELENBP1. Our data showed that selenium supplementation inhibited PAF activation induced by TGF-β in a manner dependent on elevating SELENBP1. We concluded that SELENBP1 was a key downstream target mediating the effect of selenium on PAF activation balance. This mechanism also reasonably explained the reduction of pulmonary adventitial fibrosis and vascular wall hypertrophy in MCT rats after prophylactic selenium supplementation. Our findings provided important evidence for the treatment of PAH with selenium supplementation in clinical practice.

Elucidating the mechanism by which SELENBP1 regulates PAF activation is the goal of future research. Rachedi et al.[17] demonstrated that sustaining proline synthesis was necessary for PAF activation. In this study, we preliminarily explored the potential crosstalk of the selenium-SELENBP1 axis with proline metabolism in PAF activation. We found that selenium supplementation in TGF-β stimulated PAFs could inhibit proline synthesis from glutamate and ornithine. SELENBP1 mainly inhibited proline synthesis from glutamate and mediated the effect of selenium supplementation on this pathway. Meanwhile, SELENBP1 mediated the effect of selenium supplementation on proline degradation. Future studies are needed to explore the specific regulation of proline synthesis by the axis. Based on existing literature, a recent study[28] indicated that downregulating SELENBP1 could result in the activation of cardiac fibroblasts by inhibiting the classical pathway of apoptosis. It corroborated our findings in PAFs to some extent. However, it is difficult to distinguish whether the change of apoptotic pathway is the mechanism mediating the effect of SELENBP1 or the result of fibroblast activation. Additionally, SELENBP1 has methanethiol oxidase activity, converting methanethiol to H_2O_2, formaldehyde, and H_2S.[29] The endogenous H_2O_2 and H_2S were important cell signaling molecules.[30] In multiple organ fibrosis models, endogenous H_2S antagonized fibroblast activation by reducing oxidative stress damage.[31–33] These evidences supported the hypothesis that SELENBP1 regulated the activation of PAFs by producing H_2S and other mediators. Lastly, the regulation of PAF activation by SELENBP1 may also be related to the HIF-1α pathway.[34,35]

Limitations of the study

At first, we only investigated a small sample size of PAH patients in a single center and lacked survival data for the patients. A large-scale multicenter prospective cohort with multiethnic patients should be established to confirm the association of selenium deficiency with PAH. Next, we did not systematically explore the relationship between selenium deficiency and other types of cells (such as PASMCs) and lacked a holistic understanding of selenium deficiency in PAH. Finally, we did not include *in vivo* studies of manipulating SELENBP1 expression. We will establish SELENBP1 transgenic rodent models and further clarify the mechanism of SELENBP1 regulating pulmonary circulation homeostasis.

RESOURCE AVAILABILITY

Lead contact

Further information and requests for resources and reagents should be directed to and will be fulfilled by the lead contact, Lihuang Zha (zhalihuang@csu.edu.cn).

Materials availability

This study did not generate new unique reagents.

Data and code availability

- Original proteomic data have been deposited at iProX and are publicly available as of the date of publication. All original data reported in this paper will be shared by the lead contact upon request.
- This paper does not conceive original code.
- Any additional information required to reanalyze the data reported in this paper is available from the lead contact upon request.

ACKNOWLEDGMENTS

The authors would like to express their sincere gratitude to all study participants. The authors acknowledge the support of the BioRender App, GraphPad Prism, and the Hiplot website for visualizing model diagrams and other figures. This work was supported by the National Natural Science Foundation of China (grants 82300081, 82100071, and 82070055) and the Natural Science Foundation Project of Hunan Province (grants 2024JJ6673, 2022JJ40769, 2022JJ30981, 2024JJ6620, and 2023JJ40963).

AUTHOR CONTRIBUTIONS

M.Z. and L.Z. designed the study. B.Liang and M.Z. conducted animal and cellular experiments. W.L., Y.T., and T.L. assisted in animal experiments and bioinformatics analysis. Q.C., W.Z., and X.Z. helped collect the clinical information and blood samples of the study participants. J.M. and B.Liu provided assistance in statistical analysis. B.Liang drafted the manuscript. Z.Y. critically revised the intellectual content of this work.

DECLARATION OF INTERESTS

The authors declare no competing interests.

STAR★METHODS

Detailed methods are provided in the online version of this paper and include the following:

- KEY RESOURCES TABLE
- EXPERIMENTAL MODEL AND STUDY PARTICIPANT DETAILS
  - Human participants
  - Animals
  - Primary culture of rat PAFs
- METHOD DETAILS
  - Inductively coupled plasma mass spectrometry
  - Atomic absorption spectroscopy
  - Hemodynamic evaluation in rats
  - Pathological staining and immunohistochemistry on lung sections
  - Mass spectrometry proteomics analysis
  - Transfection with siRNA or adenovirus vectors
  - Western blot analysis
  - *In vitro* scratch assay
  - CCK8 cell viability assay
  - qRT-PCR analysis
- QUANTIFICATION AND STATISTICAL ANALYSIS

SUPPLEMENTAL INFORMATION

Supplemental information can be found online at https://doi.org/10.1016/j.isci.2024.111036.

Received: January 1, 2024
Revised: June 28, 2024
Accepted: September 23, 2024
Published: September 26, 2024

REFERENCES

1. Humbert, M., Kovacs, G., Hoeper, M.M., Badagliacca, R., Berger, R.M.F., Brida, M., Carlsen, J., Coats, A.J.S., Escribano-Subias, P., Ferrari, P., et al. (2022). 2022 ESC/ERS Guidelines for the diagnosis and treatment of pulmonary hypertension. Eur. Heart J. *43*, 3618–3731. https://doi.org/10.1093/eurheartj/ehac237.
2. D'Alonzo, G.E., Barst, R.J., Ayres, S.M., Bergofsky, E.H., Brundage, B.H., Detre, K.M., Fishman, A.P., Goldring, R.M., Groves, B.M., Kernis, J.T., et al. (1991). Survival in patients with primary pulmonary hypertension. Results from a national prospective registry. Ann. Intern. Med. *115*, 343–349. https://doi.org/10.7326/0003-4819-115-5-343.
3. Boucly, A., Savale, L., Jaïs, X., Bauer, F., Bergot, E., Bertoletti, L., Beurnier, A., Bourdin, A., Bouvaist, H., Bulifon, S., et al. (2021). Association between Initial Treatment Strategy and Long-Term Survival in Pulmonary Arterial Hypertension. Am. J. Respir. Crit. Care Med. *204*, 842–854. https://doi.org/10.1164/rccm.202009-3698OC.
4. Hassoun, P.M. (2021). Pulmonary Arterial Hypertension. N. Engl. J. Med. *385*, 2361–2376. https://doi.org/10.1056/NEJMra2000348.
5. Sun, W., and Chan, S.Y. (2018). Pulmonary Arterial Stiffness: An Early and Pervasive Driver of Pulmonary Arterial Hypertension. Front. Med. *5*, 204. https://doi.org/10.3389/fmed.2018.00204.
6. Luo, Y., Dong, H.Y., Zhang, B., Feng, Z., Liu, Y., Gao, Y.Q., Dong, M.Q., and Li, Z.C. (2015). miR-29a-3p attenuates hypoxic pulmonary hypertension by inhibiting pulmonary adventitial fibroblast activation. Hypertension *65*, 414–420. https://doi.org/10.1161/hypertensionaha.114.04600.
7. Li, M., Riddle, S.R., Frid, M.G., El Kasmi, K.C., McKinsey, T.A., Sokol, R.J., Strassheim, D., Meyrick, B., Yeager, M.E., Flockton, A.R., et al. (2011). Emergence of fibroblasts with a proinflammatory epigenetically altered phenotype in severe hypoxic pulmonary hypertension. J. Immunol. *187*, 2711–2722. https://doi.org/10.4049/jimmunol.1100479.
8. Li, M., Plecitá-Hlavatá, L., Dobrinskikh, E., McKeon, B.A., Gandjeva, A., Riddle, S., Laux, A., Prasad, R.R., Kumar, S., Tuder, R.M., et al. (2023). SIRT3 Is a Critical Regulator of Mitochondrial Function of Fibroblasts in Pulmonary Hypertension. Am. J. Respir. Cell Mol. Biol. *69*, 570–583. https://doi.org/10.1165/rcmb.2022-0360OC.
9. Bertero, T., Oldham, W.M., Cottrill, K.A., Pisano, S., Vanderpool, R.R., Yu, Q., Zhao, J., Tai, Y., Tang, Y., Zhang, Y.Y., et al. (2016). Vascular stiffness mechanoactivates YAP/TAZ-dependent glutaminolysis to drive pulmonary hypertension. J. Clin. Invest. *126*, 3313–3335. https://doi.org/10.1172/jci86387.
10. Martens, P., Yu, S., Larive, B., Borlaug, B.A., Erzurum, S.C., Farha, S., Finet, J.E., Grunig, G., Hemnes, A.R., Hill, N.S., et al. (2023). Iron deficiency in pulmonary vascular disease: pathophysiological and clinical implications. Eur. Heart J. *44*, 1979–1991. https://doi.org/10.1093/eurheartj/ehad149.
11. Cuthbertson, I., Morrell, N.W., and Caruso, P. (2023). BMPR2 Mutation and Metabolic Reprogramming in Pulmonary Arterial Hypertension. Circ. Res. *132*, 109–126. https://doi.org/10.1161/circresaha.122.321554.
12. Cotroneo, E., Ashek, A., Wang, L., Wharton, J., Dubois, O., Bozorgi, S., Busbridge, M., Alavian, K.N., Wilkins, M.R., and Zhao, L. (2015). Iron homeostasis and pulmonary hypertension: iron deficiency leads to pulmonary vascular remodeling in the rat. Circ. Res. *116*, 1680–1690. https://doi.org/10.1161/circresaha.116.305265.
13. El-Kersh, K., Danielle Hopkins, C., Wu, X., Rai, S.N., Cai, L., and Huang, J. (2022). Plasma level of antimony correlates with pulmonary arterial hypertension severity. Curr. Res. Toxicol. *3*, 100080. https://doi.org/10.1016/j.crtox.2022.100080.
14. El-Kersh, K., Hopkins, C.D., Wu, X., Rai, S.N., Cave, M.C., Smith, M.R., Go, Y.M., Jones,

D.P., Cai, L., and Huang, J. (2023). Metallomics in pulmonary arterial hypertension patients. Pulm. Circ. *13*, e12202. https://doi.org/10.1002/pul2.12202.

15. Sun, Q., Hackler, J., Hilger, J., Gluschke, H., Muric, A., Simmons, S., Schomburg, L., and Siegert, E. (2020). Selenium and Copper as Biomarkers for Pulmonary Arterial Hypertension in Systemic Sclerosis. Nutrients *12*, 1894. https://doi.org/10.3390/nu12061894.
16. Stelzer, G., Rosen, N., Plaschkes, I., Zimmerman, S., Twik, M., Fishilevich, S., Stein, T.I., Nudel, R., Lieder, I., Mazor, Y., et al. (2016). The GeneCards Suite: From Gene Data Mining to Disease Genome Sequence Analyses. Curr. Protoc. Bioinformatics *54*, 1.30.1–1.30.33. https://doi.org/10.1002/cpbi.5.
17. Rachedi, N.S., Tang, Y., Tai, Y.Y., Zhao, J., Chauvet, C., Grynblat, J., Akoumia, K.K.F., Estephan, L., Torrino, S., Sbai, C., et al. (2024). Dietary intake and glutamine-serine metabolism control pathologic vascular stiffness. Cell Metab. *36*, 1335–1350.e8. https://doi.org/10.1016/j.cmet.2024.04.010.
18. Hamanaka, R.B., O'Leary, E.M., Witt, L.J., Tian, Y., Gökalp, G.A., Meliton, A.Y., Dulin, N.O., and Mutlu, G.M. (2019). Glutamine Metabolism Is Required for Collagen Protein Synthesis in Lung Fibroblasts. Am. J. Respir. Cell Mol. Biol. *61*, 597–606. https://doi.org/10.1165/rcmb.2019-0008OC.
19. Fairweather-Tait, S.J., Bao, Y., Broadley, M.R., Collings, R., Ford, D., Hesketh, J.E., and Hurst, R. (2011). Selenium in human health and disease. Antioxid. Redox Signal. *14*, 1337–1383. https://doi.org/10.1089/ars.2010.3275.
20. Rayman, M.P. (2012). Selenium and human health. Lancet *379*, 1256–1268. https://doi.org/10.1016/s0140-6736(11)61452-9.
21. Ning, Y., Hu, M., Chen, S., Zhang, F., Yang, X., Zhang, Q., Gong, Y., Huang, R., Liu, Y., Chen, F., et al. (2022). Investigation of selenium nutritional status and dietary pattern among children in Kashin-Beck disease endemic areas in Shaanxi Province, China using duplicate portion sampling method. Environ. Int. *164*, 107255. https://doi.org/10.1016/j.envint.2022.107255.
22. Kwant, C.T., van der Horst, F.A.L., Bogaard, H.J., de Man, F.S., and Vonk Noordegraaf, A. (2022). Nutritional status in pulmonary arterial hypertension. Pulm. Circ. *12*, e12173. https://doi.org/10.1002/pul2.12173.
23. Nordberg, M., and Nordberg, G.F. (2016). Trace element research-historical and future aspects. J. Trace Elem. Med. Biol. *38*, 46–52. https://doi.org/10.1016/j.jtemb.2016.04.006.
24. Kuropatkina, T., Pavlova, O., Gulyaev, M., Pirogov, Y., Khutorova, A., Stvolinsky, S., Medvedeva, N., and Medvedev, O. (2022). Sex-Dependent Protective Effect of Combined Application of Solubilized Ubiquinol and Selenium on Monocrotaline-Induced Pulmonary Hypertension in Wistar Rats. Antioxidants *11*, 549. https://doi.org/10.3390/antiox11030549.
25. Cai, C., Wu, Y., Yang, L., Xiang, Y., Zhu, N., Zhao, H., Hu, W., Lv, L., and Zeng, C. (2021). Sodium Selenite Attenuates Balloon Injury-Induced and Monocrotaline-Induced Vascular Remodeling in Rats. Front. Pharmacol. *12*, 618493. https://doi.org/10.3389/fphar.2021.618493.
26. Zhu, M.L., Gao, Z.T., Lu, J.X., Wang, Y., Wang, G., Zhu, T.T., Li, P., Liu, C., Wang, S.X., and Yang, L. (2020). Amorphous nano-selenium quantum dots prevent pulmonary arterial hypertension through recoupling endothelial nitric oxide synthase. Aging (Albany NY) *13*, 3368–3385. https://doi.org/10.18632/aging.202215.
27. Jeong, J.Y., Wang, Y., and Sytkowski, A.J. (2009). Human selenium binding protein-1 (hSP56) interacts with VDU1 in a selenium-dependent manner. Biochem. Biophys. Res. Commun. *379*, 583–588. https://doi.org/10.1016/j.bbrc.2008.12.110.
28. Shiraishi, M., Suzuki, K., and Yamaguchi, A. (2023). Effect of mechanical tension on fibroblast transcriptome profile and regulatory mechanisms of myocardial collagen turnover. FASEB J. *37*, e22841. https://doi.org/10.1096/fj.202201899R.
29. Pol, A., Renkema, G.H., Tangerman, A., Winkel, E.G., Engelke, U.F., de Brouwer, A.P.M., Lloyd, K.C., Araiza, R.S., van den Heuvel, L., Omran, H., et al. (2018). Mutations in SELENBP1, encoding a novel human methanethiol oxidase, cause extraoral halitosis. Nat. Genet. *50*, 120–129. https://doi.org/10.1038/s41588-017-0006-7.
30. Steinbrenner, H., Micoogullari, M., Hoang, N.A., Bergheim, I., Klotz, L.O., and Sies, H. (2019). Selenium-binding protein 1 (SELENBP1) is a marker of mature adipocytes. Redox Biol. *20*, 489–495. https://doi.org/10.1016/j.redox.2018.11.004.
31. Sheng, J., Shim, W., Wei, H., Lim, S.Y., Liew, R., Lim, T.S., Ong, B.H., Chua, Y.L., and Wong, P. (2013). Hydrogen sulphide suppresses human atrial fibroblast proliferation and transformation to myofibroblasts. J. Cell Mol. Med. *17*, 1345–1354. https://doi.org/10.1111/jcmm.12114.
32. Kim, J., Seok, Y.M., Jung, K.J., and Park, K.M. (2009). Reactive oxygen species/oxidative stress contributes to progression of kidney fibrosis following transient ischemic injury in mice. Am. J. Physiol. Renal Physiol. *297*, F461–F470. https://doi.org/10.1152/ajprenal.90735.2008.
33. Kalayarasan, S., Sriram, N., Soumyakrishnan, S., and Sudhandiran, G. (2013). Diallylsulfide attenuates excessive collagen production and apoptosis in a rat model of bleomycin induced pulmonary fibrosis through the involvement of protease activated receptor-2. Toxicol. Appl. Pharmacol. *271*, 184–195. https://doi.org/10.1016/j.taap.2013.04.021.
34. Jeong, J.Y., Zhou, J.R., Gao, C., Feldman, L., and Sytkowski, A.J. (2014). Human selenium binding protein-1 (hSP56) is a negative regulator of HIF-1α and suppresses the malignant characteristics of prostate cancer cells. BMB Rep. *47*, 411–416. https://doi.org/10.5483/bmbrep.2014.47.7.104.
35. Hu, C.J., Laux, A., Gandjeva, A., Wang, L., Li, M., Brown, R.D., Riddle, S., Kheyfets, V.O., Tuder, R.M., Zhang, H., and Stenmark, K.R. (2023). The Effect of Hypoxia-inducible Factor Inhibition on the Phenotype of Fibroblasts in Human and Bovine Pulmonary Hypertension. Am. J. Respir. Cell Mol. Biol. *69*, 73–86. https://doi.org/10.1165/rcmb.2022-0114OC.
36. Varghese, F., Bukhari, A.B., Malhotra, R., and De, A. (2014). IHC Profiler: an open source plugin for the quantitative evaluation and automated scoring of immunohistochemistry images of human tissue samples. PLoS One *9*, e96801. https://doi.org/10.1371/journal.pone.0096801.

STAR★METHODS

KEY RESOURCES TABLE

REAGENT or RESOURCE	SOURCE	IDENTIFIER
Antibodies		
Rabbit polyclonal anti-CD31	AiFang Biological	catalog AFW20478
Rabbit monoclonal anti-α-SMA	Proteintech	catalog 80008-1-RR; RRID: AB_2882938
Mouse monoclonal anti-vimentin	Proteintech	catalog 60330-1-Ig; RRID: AB_2881439
Rabbit polyclonal anti-SELENBP1	Abcam	catalog ab90135; RRID: AB_2042880
Rabbit polyclonal anti-Collagen Type I	Bioworld	catalog BS60771
Rabbit polyclonal anti-Collagen Type III	Proteintech	catalog 22734-1-AP; RRID: AB_2879158
Mouse monoclonal anti-PCNA	Proteintech	catalog 60097-1-Ig; RRID: AB_2236728
Mouse monoclonal anti-β-Actin	Proteintech	catalog 66009-1-Ig; RRID: AB_2687938
Bacterial and virus strains		
pAdEasy-EF1-MCS-3flag-CMV-EGFP carrying SELENBP1 expression sequence	HANBIO	N/A
Biological samples		
The venous blood samples of PAH patients and healthy volunteers	Xiangya Hospital of Central South University	N/A
Chemicals, peptides, and recombinant proteins		
Monocrotaline	Sigma-Aldrich	catalog C2401
Selenium yeast tablets	Yinnuoke Pharmaceutical Corp.	catalog H20084125
Amobarbital	Sigma-Aldrich	catalog 1030001
Fibroblast growth supplement	ScienCell	catalog 2352
Recombinant transforming growth factor β	PeproTech	catalog 100-21
Sodium selenite	Sigma-Aldrich	catalog 214485
Phosphatase Inhibitor Cocktail	TOPSCIENCE	catalog C0002
Protease Inhibitor Cocktail	TOPSCIENCE	catalog C0001
RIPA buffer	Epizyme	catalog PC105
Critical commercial assays		
Hematoxylin and eosin staining kit	Biosharp	catalog BL700A
Masson's trichrome staining kit	Solarbio	catalog G1340
Elastica van Gieson staining kit	Leagene Biotechnology	catalog DC0064
Goat anti-mouse/rabbit IgG polymer	ZSGB-BIO	catalog PV-9000
Diaminobenzidine staining kit	ZSGB-BIO	catalog ZLI-9018
BCA kit	Epizyme	catalog ZJ102
CCK8 kit	NCM Biotech	catalog C6005
RNA extraction kit	OMEGA biotek	catalog 6834
Surescript first-strand cDNA synthesis kit	GeneCopeia	catalog QP056
Blazetaq probe qPCR mix	GeneCopeia	catalog QP036
Deposited data		
Proteomic data of pulmonary artery branches in MCT rats versus control rats	This paper	iProX database: IPX0009780000
Experimental models: Cell lines		
Primary cultured rat pulmonary adventitial fibroblasts	This paper	N/A

(*Continued on next page*)

Continued

REAGENT or RESOURCE	SOURCE	IDENTIFIER
Experimental models: Organisms/strains		
Sprague Daley rats	Slake Jingda Corp.	N/A
Oligonucleotides		
siRNA targeting sequence: SELENBP1 5′-GCTGTATGGGAGCCACATA-3′	RIBOBIO	N/A
Primer: ACTB F: 5′-TAAGGCCAACCGTGAAAAGATG-3′; R: 5′-GTACGACCAGAGGCATACAGG-3′	This paper	N/A
Primer: OAT F: 5′- CCAGTTCCACAGATCCGACC-3′; R: 5′- GGATGGGCTCCACCATGAAA-3′	This paper	N/A
Primer: P5CS F: 5′- TCCTGACTGTCTACCCCAGG-3′; R: 5′- CAGGAGGTGAAGAATGCGGT-3′	This paper	N/A
Primer: PYCR1 F: 5′- CCCTGCTTATCAATGCTGTGG-3′; R: 5′- GAGGAGTCTAGCTTCACCTTGT-3′	This paper	N/A
Primer: PYCR2 F: 5′- GTTGCTGGGAGCAGCTAAGA-3′; R: 5′- GAGGGTCTTCTTAAGGGCGG-3′	This paper	N/A
Primer: PYCR3 F: 5′- CTATGGAGGAGCTGTTACCCC-3′; R: 5′- GTTCTGTAGGAGCTTGGCGT-3′	This paper	N/A
Primer: ALDH4A1 F: 5′- TCTCCCTTCAACTTCACCGC-3′; R: 5′- GTGACTGTGTCCCCGAATGT-3′	This paper	N/A
Primer: PRODH2 F: 5′- TGGATGTGCTGGCCAAGGTA-3′; R: 5′- TATCCACATTGAACCTGCGCT-3′	This paper	N/A
Software and algorithms		
GeneCards database	Stelzer et al.[16]	https://genecards.org/
ImageJ	Varghese et al.[36]	https://imagej.net/
Hiplot Pro platform	Shanghai Tengyun Biotechnology Co., Ltd.	https://hiplot.com.cn/
GraphPad Prism	Dotmatics Co., Ltd.	https://graphpad.com
BioRender App	BioRender Co., Ltd.	https://app.biorender.com/
Adobe Illustrator	Adobe Systems Co., Ltd.	https://adobe.com/

EXPERIMENTAL MODEL AND STUDY PARTICIPANT DETAILS

Human participants

The clinical characteristics of all participants have been described in Tables S1 and S2. The investigators obtained informed consent from the participants and ethical approval from the ethics committee of Xiangya Hospital of Central South University. All research procedures conformed to the declaration of Helsinki. This study included PAH patients ≥ 18 years old who visited Xiangya Hospital from 2020 to 2022. Their mean pulmonary arterial pressure at rest was ≥ 20mmHg confirmed by right heart catheterization. The control population was age- and gender-matched healthy volunteers who came to Xiangya Hospital for physical examination. All human venous blood samples were collected into the blood collection tubes containing coagulant at the first visit of the participants and then were centrifuged for 15 min (3000r/min) to obtain enough serum.

Animals

The animal experimental protocol followed the NIH guideline for the care and use of laboratory animals and was approved by the laboratory animal welfare and ethics committee of Central South University. 8-week male Sprague Daley rats were purchased from Slake Jingda Corp. and raised in a specific pathogen-free environment, with a temperature of 22 ± 3°C, 12h cycle of day and night, and free access to food and water.

Experimental scheme 1: After adaptive feeding for 1 week, 25 rats were randomly divided into 3 groups: control (n=7), MCT (n=9), and MCT+Se (n=9) groups. Rats in MCT and MCT+Se groups received MCT (Sigma-Aldrich, catalog C2401) 60mg/kg body weight intraperitoneally to induce pulmonary hypertension. Rats in the control group received an equal volume of physiological saline intraperitoneally. The selenium yeast tablets (Yinnuoke Pharmaceutical Corp., catalog H20084125) were completely ground and dissolved to make a selenium solution with a content of 5 mg/l. At the same time of MCT administration, the water of rats in the MCT+Se group was replaced with the selenium

solution to supplement selenium. There was no significant difference in water consumption of each cage. On the 21st day after MCT administration, the rats were anesthetized with amobarbital (Sigma-Aldrich, catalog 1030001) 30mg/kg body weight and then sacrificed after receiving hemodynamic evaluation. The lung and heart tissues of the rats were collected rapidly. The heart was dissected into left ventricle + interventricular septum and right ventricular free wall, and the RVHI was calculated according to the weight of right ventricle/left ventricle + interventricular septum to evaluate the level of right heart remodeling.

Experimental scheme 2: 6 Sprague Daley rats were randomly divided into control group (n=3) and MCT group (n=3). They were injected with MCT or an equal volume of saline according to the above method. After establishing models, the pulmonary artery branches below grade 3 of the rats were carefully stripped, rinsed with sterile saline on ice, and frozen with liquid nitrogen for proteomic analysis.

Primary culture of rat PAFs

After euthanasia, the pulmonary artery branches below grade 3 of healthy rats were carefully stripped and cut into tissue blocks of about $1mm^2$ in size to attach to the bottom of T25 culture flasks. 5ml of DMEM/F-12 medium containing 20% fetal bovine serum and 1% antibiotic/antimycotic was added along the lateral wall when the tissue block was slightly dry. After 3-5 days of primary culture, the cells migrated out of the tissue blocks and fused. The cells were digested and re-adherent for 30 min, and then the medium was replaced to remove impurities such as suspended smooth muscle cells. The adherent PAFs were grown in DMEM/F-12 medium containing 5% fetal bovine serum, 1% antibiotic/antimycotic, and 1% fibroblast growth supplement (ScienCell, catalog 2352) at 37°C and 5% CO_2. The purity of PAFs was determined by observing the in-situ expression of cell markers through cellular immunofluorescence, including CD31 (1:200, AiFang Biological, catalog AFW20478), α-SMA (1:200, Proteintech, catalog 80008-1-RR; RRID: AB_2882938), and Vimentin (1:200, Proteintech, catalog 60330-1-Ig; RRID: AB_2881439). The PAFs with purity ≥ 95% at passages 3-6 were used for subsequent experiments. Recombinant TGF-β (10 ng/ml for 24 h, PeproTech, catalog 100-21) was used to establish PAH-related PAF *in vitro* models. Sodium selenite (2nM for 24h, Sigma-Aldrich, catalog 214485) was added to the medium to supplement selenium *in vitro*.

METHOD DETAILS

Inductively coupled plasma mass spectrometry

For the discovery cohort, ICP-MS (Thermo Fisher Scientific) was used to measure the contents of 34 ions in human serum samples. Firstly, 100ul of serum was mixed with 1ml of concentrated nitric acid solution, and digested at 65°C for 4 h. Then deionized water was added to the solution to make its volume reach 20ml. Meanwhile, 8 tubes of nitric acid solution with the same concentration as the samples were prepared as the blank sample for determination. Finally, the samples were tested on the ICP-MS with the blank value correction before each batch of tests. Selenium content was normalized to the certified reference value.

Atomic absorption spectroscopy

For the validation cohort and rat models, atomic absorption spectroscopy (Varian) was used for the relative quantitative analysis of selenium. 500ul of serum or 50mg lung tissue and fresh hydrochloric acid perchloric acid mixture were completely mixed and digested for 1 h. The reducing agent (2% potassium borohydride solution) was added to the samples, and then the volume was fixed to 25ml with deionized water. After the machine was calibrated, the selenium standard samples were detected first to draw a standard curve. The prepared samples were measured, and the results were normalized to the certified reference value.

Hemodynamic evaluation in rats

After anesthesia, a polyethylene catheter was inserted into the right external jugular vein of the rat, one end of which was placed in the right ventricle, and the other end was connected with a pressure transducer. The RVSP was recorded by the biological signal acquisition and processing system (TECHMAN) and analyzed based on the built-in program.

Pathological staining and immunohistochemistry on lung sections

The middle lobe of the rat's right lung was fixed with 4% paraformaldehyde and embedded in paraffin to prepare 5mm serial sections. The sections were stained with hematoxylin and eosin (Biosharp, catalog BL700A) to show the morphology of pulmonary arterioles. According to the manufacturer's instructions, the sections were stained with Masson's trichrome (Solarbio, catalog G1340) to show the level of pulmonary arteriole fibrosis. The collagen volume fraction was represented as the percentage of collagen-positive blue area to the total area of pulmonary arterioles, which was calculated by ImageJ. Generally, the collagen volume fraction of each sample was averaged from at least 20 images. Elastica van Gieson staining and immunohistochemical staining of α-SMA were performed to evaluate the media hypertrophy of pulmonary arterioles. The former was conducted according to the protocol provided by the manufacturer (Leagene Biotechnology, catalog DC0064), which demonstrated the black inner and outer elastic plates as well as the yellow media in the middle. For immunohistochemistry, dewaxed lung sections were heated in 10 mmol/l citric acid buffer (pH=6) for antigen retrieval, and then endogenous peroxidase activity was blocked. The sections were blocked and permeabilized with 3% bovine serum albumin + 0.3% TritonX-100 solution for 1 h at room temperature. At 4°C, the sections were incubated with α-SMA (1:200, Proteintech, catalog 80008-1-RR; RRID: AB_2882938) or SELENBP1 (1:200, Abcam, catalog ab90135; RRID: AB_2042880) specific antibody for 12 h, followed by goat anti-mouse/rabbit IgG polymer (ZSGB-BIO, catalog PV-9000) for 1 h at 37°C. The protein expression was then shown by diaminobenzidine staining (ZSGB-BIO, catalog ZLI-9018). Images were acquired by microscope (Leica) and

analyzed by ImageJ. The vascular media hypertrophy was represented as (arteriole diameter-lumen diameter)/arteriole diameter*100%, which was calculated based on α-SMA stained images. At least 20 images were averaged for the vascular media hypertrophy of each sample. With the help of the IHC Profiler plug-in component in ImageJ,[36] SELENBP1 staining intensity of pulmonary arterioles was defined as the percentage contribution of positive. The percentage contribution of positive in each sample was an average of at least 20 images.

Mass spectrometry proteomics analysis

The proteins were extracted from the pulmonary arteries of MCT or control rats in animal experimental scheme 2 and digested into polypeptide mixtures. The subsequent liquid chromatography coupled to tandem mass spectrometry (LC-MS/MS) analysis and tandem mass tag (TMT)-labelled quantitative proteomics were carried out by Applied Protein Technology Corp. The presence of a protein was defined as being identified at least 2 times in 3 biological replicates. The differentially expressed proteins were selected according to the criteria of fold change ≥ 1.2 or ≤ 0.83, and $p<0.05$.

Transfection with siRNA or adenovirus vectors

To manipulate the expression of SELENBP1, we commissioned the manufacturers to design specific siRNA sequences (RIBOBIO, 5′-GCTGTATGGGAGCCACATA-3′) and adenovirus vectors carrying SELENBP1 expression sequence (HANBIO). Correspondingly, negative control siRNA and empty adenovirus vectors were used for the control group. The transfection of siRNA was performed according to the instructions of RIBOBIO, and the concentration of 100nM was appropriate. The optimal multiplicity of infection of adenovirus vectors was 20.

Western blot analysis

Total proteins of lung tissues and cells were extracted through RIPA buffer (Epizyme, catalog PC105) with 1% protease inhibitors and phosphatase inhibitors (TOPSCIENCE, catalog C0001). The concentration of protein was determined using BCA Kit (Epizyme, catalog ZJ102). Briefly, the quantified samples of each group were loaded on SDS-PAGE gels and then transferred to a polyvinylidene difluoride membrane. After blocking with 5% bovine serum albumin solution, the membrane was incubated with specific antibodies of SELENBP1 (1:1000, Abcam, catalog ab90135; RRID: AB_2042880), Collagen Type I (1:500, Bioworld, catalog BS60771), Collagen Type III (1:500, Proteintech, catalog 22734-1-AP; RRID: AB_2879158), α-SMA (1:5000, Proteintech, catalog 80008-1-RR; RRID: AB_2882938), or PCNA (1:5000, Proteintech, catalog 60097-1-Ig; RRID: AB_2236728) for 12 h at 4°C. β-actin (1:5000, Proteintech, catalog 66009-1-Ig; RRID: AB_2687938) was adopted as an internal reference. After incubation with HRP-conjugated secondary antibodies (1:2500, Proteintech, catalog SA00001-1 or SA00001-2) for 1 h at room temperature, the reaction bands were visualized on a chemiluminescence instrument (Bio-Rad) and quantitatively analyzed by ImageJ.

In vitro scratch assay

To assess the migration ability of PAFs, the cells were scratched after specific treatments (such as transfection of siRNA) and cultured in the medium without fetal bovine serum. The images immediately acquired by an inverted microscope (Leica) were recorded as 0 h images. After 24 h of culture, the cell plates were located at the same position and 24 h images were taken. The migration rate was represented as the percentage of the reduction of the same scratch width from 0 h to 24 h.

CCK8 cell viability assay

To preliminarily explore the effect of selenium supplementation on PASMCs, the cells were treated with PDGF or PDGF+selenium supplementation. After 24h, the cells were incubated with CCK8 reagent (NCM Biotech, catalog C6005) at 37°C for about 1h and detected the absorbance at the wavelength of 450nm to observe the changes of cell viability.

qRT-PCR analysis

The lung tissue and cells were homogenized using RNA extraction kit (OMEGA biotek, catalog 6834), and mRNA was isolated. cDNA was then reverse transcribed using the surescript first-strand cDNA synthesis kit (GeneCopeia, catalog QP056). Finally, The target genes in the cDNA samples were quantified using blazetaq probe qPCR mix (GeneCopeia, catalog QP036) on QuantStudio 5 (Thermo Fisher Scientific). The relative mRNA levels of these genes were calculated by $2^{-\Delta\Delta}$ CT method with ACTB as internal reference. The primers were described in the key resources table.

QUANTIFICATION AND STATISTICAL ANALYSIS

All data had three or more biological replicates. Shapiro-Wilk test was used to estimate whether the data conformed to normal distribution. Continuous variables were presented as mean±SEM if normal distribution were satisfied, or as median (interquartile range) otherwise. Continuous variables were compared by unpaired student's t-test or Mann-Whitney U test. Categorical variables were presented in the form of the number of cases (percentage), and the difference was compared by chi-square test or Fisher's exact test. Linear regression analysis was conducted to explore the association between selenium content and patients' prognosis. The data were visualized in the GraphPad Prism and Hiplot platform (https://hiplot.com.cn/). The above statistical analyses were performed in GraphPad Prism. $p<0.05$ (two-sided) was considered statistically significant.